Journal of Materials Chemistry

Cite this: *J. Mater. Chem.*, 2012, **22**, 17311

www.rsc.org/materials

PAPER

Characterization and drug release behavior of highly responsive chip-like electrically modulated reduced graphene oxide–poly(vinyl alcohol) membranes†

Heng-Wen Liu, Shang-Hsiu Hu, Yu-Wei Chen and San-Yuan Chen*

Received 3rd May 2012, Accepted 3rd July 2012
DOI: 10.1039/c2jm32772d

Hybrid hydrogel membranes composed of reduced graphene oxide (rGO) nanosheets and a poly (vinyl alcohol) (PVA) matrix were investigated as an electrically responsive drug release system. The rGO nanosheets in the matrix act as a physical barrier to inhibit the release of the model anesthetic drug, lidocaine hydrochloride, but the highly responsive release can be enhanced by the presence of rGO when exposed to an electrical stimulus. More interestingly, the on-demand drug release profiles of the assembled rGO–PVA hydrogel into a chip-like device can be highly controlled by an external electrical field. Release profiles ranging from a slow-elution pattern to a rapid release under electrical field treatment can be achieved by manipulating the rGO–PVA composition. Moreover, under cyclic exposure to an electrical stimulus, a highly controllable and repeatedly pulsatile release with desirable precision is obtained from the rGO–PVA hydrogel, implying that the hydrogel exhibits excellent anti-fatigue properties. By combining with the enhanced structural integrity and biocompatibility, the electrically responsive rGO–PVA hydrogel has demonstrated potential biological applications in drug delivery systems. In addition, the easy loading of hydrophilic drugs into the rGO–PVA hydrogel opens up a promising future in biological applications, such as transdermal therapy and wound healing.

1. Introduction

An environmentally sensitive drug delivery system that releases the desired concentration of a drug at the optimal time to enhance the therapeutic efficacy and decrease undesired side effects, has been recognized as a promising biomedical technology for treating diseases. Various drug delivery systems can control the release of a drug by applying an external stimulus, such as pH,[1] magnetic field,[2] and electric field.[3,4] Of these systems, electrically controlled drug delivery systems may offer unique advantages for providing the on-demand release of drugs to reach a rapid and efficacious therapy by power supply equipment. Furthermore, when combined with a sensor or microchip, feedback and remote control of the device outside the body becomes possible.

Electro-conductive hydrogels, generally consisting of an inherently conducting polymer within a polymer-based hydrogel, have been studied intensively in a wide variety of applications, such as artificial muscles,[5] biosensors,[6] and drug delivery systems.[7,8] Drug delivery systems can provide the on-demand release of drugs in response to environmental stimuli using different mechanisms, such as swelling and erosion.[9] Despite the advantageous properties, electro-conductive hydrogels also present several limitations. For example, because they are usually prepared from polyelectrolytes, most electrically responsive hydrogels cannot be used for clinical applications due to their unstable structure following electric stimulation.[10,11] To overcome these limitations, an inorganic phase, such as montmorillonite (MMT),[12] silica, or a crosslinker,[13] has been incorporated into the hydrogel matrix to enhance its mechanical properties. However, the incorporation of an inorganic phase into the hydrogel may induce toxicity and slow the electrical response in controlled drug delivery systems.[14] The practical limitations of using a hydrogel-based drug delivery may be overcome by the introduction of reduced graphene oxide (rGO).

Recently, graphite oxide and graphene-based polymer nanocomposites, such as rGO–PVA hybrid systems, have received attention in the field of materials chemistry. Further studies demonstrated the pH-sensitive,[15] antibacterial,[16] thermal, mechanical,[17] and electrical properties[18] of graphene-based polymer nanocomposites. However, up to now, the remarkable electrical characteristics of graphene-based polymers in biological applications has not been previously reported *in vitro*. In this study, lidocaine hydrochloride, which is a water-soluble drug and is commonly used as a local anesthetic to relieve pain in the clinic, was selected as a model drug. The rGO–PVA hydrogels were

Department of Materials Sciences and Engineering, National Chiao Tung University, No. 1001 Ta Hsueh Rd., Hsinchu, Taiwan 300, R.O.C. E-mail: sanyuanchen@mail.nctu.edu.tw; Fax: +88 63-5724727; Tel: +88 63-5731818

† Electronic supplementary information (ESI) available. See DOI: 10.1039/c2jm32772d

used as drug reservoirs, and the electrically stimulated drug release behavior of the rGO–PVA hydrogels for on-demand electrically responsive drug delivery systems were examined. Because rGO can serve as a percolating pathway for transferring electrons and enhancing drug release when an electric voltage is applied, the rGO-based nanocomposite can release a precisely controlled amount of drug on-demand. Furthermore, the responsiveness of the rGO–PVA hybrid hydrogel was investigated when subjected to repeated on–off switching operations. The release of lidocaine hydrochloride can be controlled for relieving the pain to specific areas as the pain occurs. By tuning the composition of the hybrid system designed in this study, a number of electrically modulated drug release profiles ranging from slow-elution to rapid-release patterns can be achieved.

2. Materials and methods

2.1. Materials

Graphite with an average mesh size of 325 and a purity of 99.8 mol% was supplied by Alfa Aesar. Concentrated sulfuric acid (95–97 mol% H_2SO_4) and phosphate-buffered saline (PBS) (pH = 7), used for the preparation of buffers, were purchased from the Sigma-Aldrich Co. Nitric acid (69–70 mol% HNO_3) and potassium chlorate were purchased from J. T. Baker. Lidocaine hydrochloride (M_W = 270.2 g mol^{-1}, pK_a = 7.9, Sigma-Aldrich Co.) was used as the model drug to characterize the release behavior of the hydrogels. Dimethyl sulfoxide (DMSO), hydrazine hydrate (80 mol%), and PVA (M_W = 78 000 g mol^{-1}, 99.7 mol%) were obtained from the Sigma-Aldrich Co. Highly electrically conductive indium-tin-oxide thin films from the Join Well Tech. Co., Ltd. were used as electrodes to stimulate the release of the drugs electrically.

2.2. Preparation of rGO–PVA composites

Graphite oxide (GO) was prepared from natural graphite powder by oxidation with potassium chlorate according to the modified Hummers' method.[19] Graphene nanosheets, and reduced graphene oxide (rGO), were generated using hydrazine hydrate. The reduction from GO was carried out at 95 °C for 2 h, and the wet rGO was isolated after centrifugation and washing with deionized water. To interpolate rGO with PVA, the following synthesis procedure to generate different composition ratios of rGO–PVA hybrid hydrogels was used: for example, PVA (3 g) was dissolved in DMSO (30 ml) at 120 °C and the solution was subsequently cooled to room temperature. After rGO (0.1 g) was added into the above solution (5 ml), the mixtures were sonicated for one hour at room temperature to produce a completely homogeneous solution. This rGO–PVA solution was poured into a 10 cm Petri dish and was subjected to freezing–thawing cycles of −4 °C for 12 h and 25 °C for 3 h. The hydrogel membrane was peeled off the substrate and was rinsed with DI water to remove any residual DMSO. Meanwhile, rGO–PVA hydrogels using different amounts of rGO loadings (0 g, 0.2 g, 0.3 g, 0.4 g, and 0.5 g) were prepared using the same procedure. The hydrogels were dried at 25 °C for 24 h to allow film formation.

2.3. Characterization

The appearance and morphology of the hydrogels were examined using scanning electron microscopy (S6700, JEOL, Japan). The topography and size of the rGO nanosheets were imaged using atomic force microscopy (AFM, diInnova™, Veeco). The UV-vis absorption spectrophotometer (Evolution 300, Thermo) set at 262 nm was used to quantify the amount of lidocaine hydrochloride released.

Moreover, the dynamic weight-loss test for the hydrogels was conducted using a thermogravimetric analyzer (DuPont 2050), which simultaneously measures the ratio of organic/inorganic material. All tests were conducted in a flowing N_2 atmosphere (60 ml min^{-1}) using samples weighing 3–5 mg and a temperature ranging from 30 °C to 800 °C at a scan rate of 10 °C min^{-1}. The tensile mechanical properties of the rGO–PVA hydrogels were measured using a complete MTS Tytron 250 and TestStar IIs system under the following conditions: crosshead speed: 10 mm min^{-1}; test temperature: 25 °C and initial cross-section :10 mm^2. Raman spectra were recorded from 1000 to 3000 cm^{-1} with Ar laser excitation at 514.5 nm. A DC power supply (Instek, Model: GPC-3030DQ) was used to electrically stimulate the drug release. All results reflect the average of three measurements, and the difference between each measurement is <5%.

The dried hydrogel without loading drug was swollen in 50 ml PBS (pH = 7) until equilibrium. After the excessive surface water had been removed using filter paper, the weight of the swollen samples was measured. The water uptake of the samples was estimated by measuring the change in the sample weight before and after immersion in PBS. The procedure was repeated three times until no further weight gain was detected. The water uptake was determined according to the following equation:

$$\text{Water uptake (\%)} = [(W_s - W_d)/W_d] \times 100$$

where W_s and W_d represent the weight of the swollen and dried samples, respectively. All results reflect the average of three measurements. The measurement error was estimated at <5%.

2.4. Drug release under an applied voltage

For the drug release test, the dried membranes were soaked in a solution of 1% lidocaine hydrochloride in water to allow the impregnation of the hydrogel with the lidocaine hydrochloride solution. The drug-loaded rGO–PVA hydrogel membrane, pre-equilibrated and washed in 50 ml PBS for 5 min, was cut into small rectangular sections (1 cm [length] × 1 cm [wide] × 0.1 cm [thick]), was weighed, and was placed into a transparent plastic container for later release experiments. The transparent plastic container, made of poly(methyl methacrylate) (PMMA, Yeongshin Co., Ltd., Taiwan), measured 2 cm (length) × 2 cm (wide) × 0.2 cm (thick) and contained a single small opening of 0.2 mm in diameter on one side of the container, whereas the other three sides of the PMMA container were mechanically sealed. The small opening is the outlet for drug elution. Rectangular ITO (two, each measuring 4 cm × 2 cm × 0.1 mm) were placed at a constant distance of 0.5 mm on two parallel sides of the acrylic container as electrodes. The hydrogel membrane was inserted into the container to form a chip-like structure and was exposed to an electric voltage, generated by a DC power source, of 2 V,

5 V, 10 V, or 15 V across the ITO electrodes in 50 ml PBS (pH = 7) for electrical stimulation. For on–off switching operations, the drug-loaded rGO–PVA hydrogel in PBS was kept in contact with the two ITO electrodes for electrostimulation under an input voltage of 15 V. A cyclic switching operation was carried out for five on–off cycles with a time interval of 5 min for each. The released amount of lidocaine hydrochloride drug was measured using a UV spectrophotometer at a specific wavelength ($\lambda = 262$ nm) at various time intervals. The obtained values are an average of three measurements and the difference between each measurement is <5%.

2.5. Cell culture

The 3-(4,5-dimethylthiazol-2-yl)-2,5-diphenyltetrazolium bromide (MTT) assay was used to determine the cytotoxicity of PVA, rGO–PVA, and rGO. WS1 cells (human skin fibroblastoids) were maintained in DMEM (Dulbecco's modified Eagle's medium) containing 10% fetal bovine serum, 100 units ml^{-1} penicillin, and 100 μg ml^{-1} streptomycin. The cells were cultured in complete medium at 37 °C in a humidified atmosphere of 5% CO_2 in air. For all experiments, the cells were harvested from subconfluent cultures using trypsin and were resuspended in fresh complete medium before plating. The *in vitro* cytotoxicity of PVA, rGO–PVA, and rGO on the WS1 cells was performed at different concentrations and times. Briefly, 1×10^5 cells were plated in 96-well plates in 1 ml culture medium and the cells were incubated with PVA, rGO–PVA, and rGO solutions at an optimal concentration of 6.25 mg ml^{-1} at 37 °C for 6 h, 12 h, or 24 h. At the end of the incubation, 20 μg of MTT solution was added and the samples were incubated for 4 h. Next, the medium was replaced with 200 μg of DMSO, and the absorbance was monitored using a Sunrise absorbance microplate reader (CTECAN) at a wavelength of 570 nm. The optical density of the media was proportional to the number of viable cells. All experiments were repeated at least three times.

3. Results and discussion

3.1. Structural characterization

Fig. 1 illustrates schematically the preparation procedures and the electrically controlled drug release from the rGO–PVA hydrogel. The rGO–PVA solution was poured into a 10 cm Petri dish and subjected to freezing–thawing cycles between −4 °C for 12 h and 25 °C for 3 h. During the cycle process, the formulation of the hydrogen bonding can be promoted at −4 °C in DMSO and then heated at 25 °C for 3 h to avoid freezing. This synthesis method produces stable hydrogels and enhances their mechanical properties due to crystalline regions[20] in the gel, which differs from other methods in which the rGO–PVA hydrogels are dried at a higher temperature under vacuum.[21–24] Furthermore, the synthesized rGO–PVA hydrogel exhibits highly flexible properties as shown in the inset in Fig. 2(a).

The PVA hydrogel used in this study is based on its biocompatibility, hydrophilic behavior, and its semi-crystalline and nonionic properties. Moreover, PVA can interact with graphene oxide by interchain hydrogen bonding[21] and acts as a model for understanding the interaction of rGO with other polar polymers. These specific properties make PVA an excellent candidate for numerous applications and it is particularly useful for rGO–hydrogel-based electrically responsive drug delivery systems. The rGO–PVA hydrogels were employed as a drug reservoir to study drug release behavior and the responsiveness to external stimulus.

Table 1 shows the composition and properties of the rGO–PVA hydrogels. The inorganic/organic ratio represents the amounts of rGO and PVA added during synthesis of the hydrogels. The actual rGO content in the PVA matrix was calculated using TGA and is shown in the ESI in Fig. S1.† The TGA curves drop rapidly at 300–400 °C and then level out at temperatures higher than 500 °C, which illustrates that the PVA matrix was totally decomposed and the residue at 500–600 °C was considered to be rGO. Therefore, the inorganic rGO content in each hydrogel can be calculated. Fig. S2† shows the relationship between rGO loading and tensile strength of the hybrid nanocomposites. It is obvious that the addition of rGO into the polymer matrix has a significant influence on its mechanical behavior. The tensile strength of sample R0 (no rGO) is only 4.17 MPa, whereas the R1 composite (containing 8.11% rGO) is 8.09 MPa; *i.e.*, the addition of rGO increased the tensile strength of pure PVA by 94%. Therefore, increasing the rGO nanosheet loading enhances the mechanical strength of the nanocomposites.

The water uptakes of the hydrogels containing different amounts of rGO are listed in Table 1. The table indicates that hydrogels R0, R1, R2, R3, R4, and R5 (containing rGO concentrations of 0.63%, 8.11%, 16.87%, 25.74%, 34.99%, and 43.47%, respectively, and constant PVAs) exhibit decreasing water uptake of 333.3%, 294.1%, 268.6%, 243.5%, 217.8% to 192.2% in 24 h, respectively. The restrained water uptake behavior of the hydrogels is attributed to the increased concentration of rGO, which suppresses the development of mesh size among the PVA chains, acts as a physical barrier and in turn affects the subsequent drug release. The amount of drug-loading by the hydrogels is also listed in Table 1, which shows that an increase in the amount of rGO in the hydrogel results in an increase in the amount of drug molecules encapsulated.[25,26] The differences in the drug-loading ability of the hydrogels is attributed to the intermolecular interactions of rGO and lidocaine hydrochloride, such as hydrogen bonding and π–π stacking, which form between the aromatic rings of rGO and the aromatic rings of lidocaine hydrochloride. In addition, the –CONH groups of lidocaine hydrochloride can form hydrogen bonds with the –OH of PVA. This finding indicates that for the rGO–PVA hydrogel, the non-covalent bonding of the drug to the rGO sheets and their trapping in the PVA matrix can increase the loading capacity of the hydrophilic drug (lidocaine hydrochloride).

Fig. 2(a) shows the SEM images of the synthesized reduced graphene oxide (rGO), which randomly aggregated with an average width ranging from 250 μm to 300 μm. In Fig. S3,† the AFM images show that the rGO height ranges from 5–10 nm and the width is approximately 300 μm, which corresponds to the SEM image of rGO. The layers are slightly thicker than the individual graphene, which is related to the aggregation due to strong van der Waals interactions between the graphene nanosheets. Fig. 2(b) shows the Raman spectra for the characterization of pristine graphite, selected GO and the rGO. The Raman

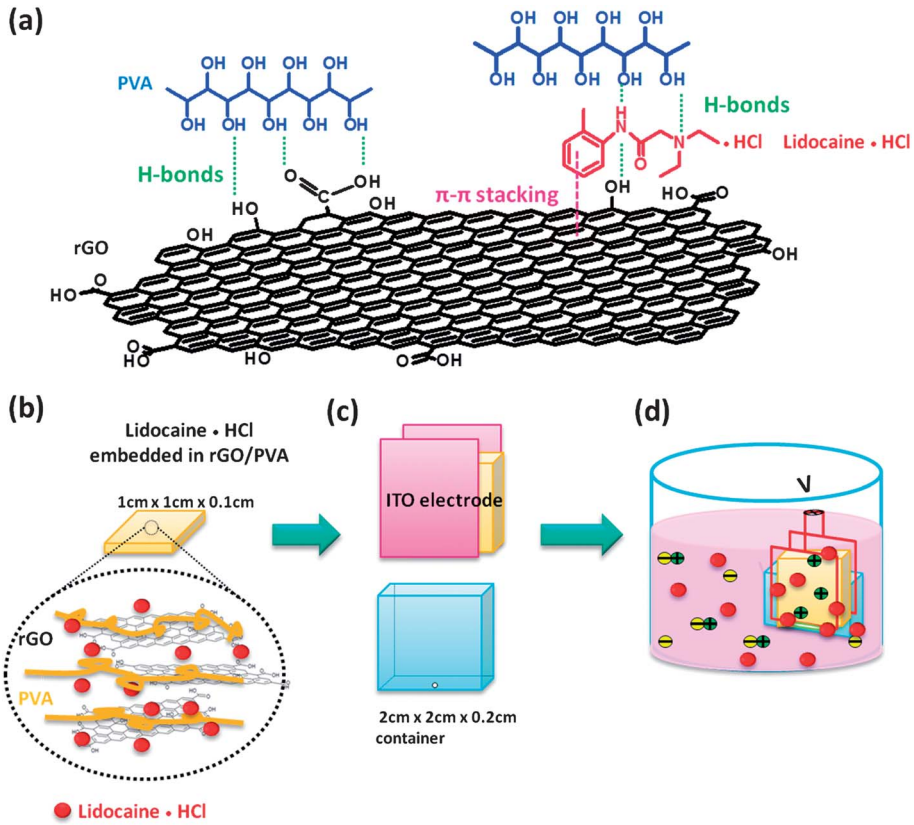

Fig. 1 Schematic diagram illustrating the synthesis of the rGO–PVA hydrogel and the electrically controlled drug release (a) structural profile of rGO intercalated with PVA and loaded with lidocaine hydrochloride. (b) The hydrogel was cut into sections measuring 1 cm × 1 cm × 0.1 cm. (c) Procedures for the preparation of the drug delivery chip-like structure. (d) The setup of the hydrogel structure; electrical fields of different strengths can be applied between the ITO electrodes in the sealed container for the controlled release of drug molecules. All data shown represent the average value of three measurements and the measurement error is well below 5%.

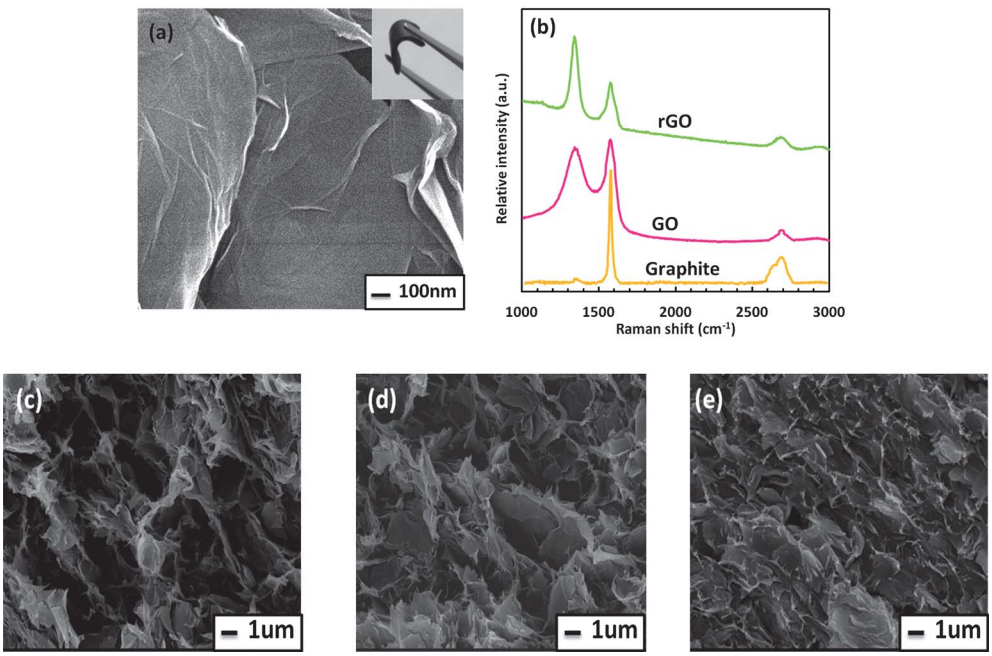

Fig. 2 (a) Scanning electron micrograph of the reduced GO, the inset demonstrates the highly flexible hydrogel. (b) The Raman spectra of graphite, GO, and the reduced GO. (c), (d), and (e) scanning electron micrographs of the cross-section rGO–PVA hydrogels with rGO contents of 8.11%, 25.74%, and 43.47%, respectively, after freeze-drying.

Table 1 Composition and properties of rGO–PVA hydrogels

Hydrogel	rGO : PVA	Inorganic rGO (wt%)[a]	Water uptake (wt%)[b]	Drug loading (%)[c]
R0	0 : 5	0.63	333.3	0.393
R1	1 : 5	8.11	294.1	0.405
R2	2 : 5	16.87	268.6	0.437
R3	3 : 5	25.74	243.5	0.450
R4	4 : 5	34.99	217.8	0.468
R5	5 : 5	43.47	192.2	0.479

[a] The rGO wt% was conducted through thermogravimetric analysis (TGA) after the rGO–PVA hydrogels were synthesized. [b] The water uptake ratio was measured by the change of sample weight before and after immersion in PBS (pH = 7). [c] The drug loading was tested by soaking in 1 wt% lidocaine hydrochloride solution.

spectrum of the pristine graphite, as expected, displays a prominent G peak at 1563 cm^{-1}, which is due to sp^2-hybridized carbon–carbon bonds,[27] and a very weak band at 1354 cm^{-1} (D band). The G band and the D band are respectively attributed to the first-order scattering of the E_{2g} vibration mode in the graphite sheets and structural defects (disorder-induced modes). The D band and the G band are also observed for GO and rGO. In the Raman spectrum of GO, the G band at 1575 cm^{-1} is broadened, the D band at 1344 cm^{-1} becomes prominent and the 2D band appears at 2674 cm^{-1}, which is the overtone (second harmonic) of the D band. For the rGO sample, the Raman spectrum also contains D, G, and 2D bands at 1340, 1575, and 2684 cm^{-1}, respectively. The ratios of D- to G-band intensity (I_D/I_G) increase from 0.43 for pristine graphite to 0.96 and 1.22 for GO and rGO, respectively. The increase of I_D/I_G indicates the decrease in the size of the in-plane sp^2 domains, possibly due to the extensive oxidation and the number of defects.[23] Therefore, the intensity ratio of D band/G band of rGO is higher than that of GO, which suggests that the sp^2 domains decreased in rGO. As explained by Stankovich *et al.*,[28] the reduced state increases the number of aromatic domains of a smaller overall size in rGO, leading to an enhancement of the I_D/I_G ratio. Fig. 2(c)–(e) show a set of SEM cross-section micrographs of the rGO–PVA hydrogels with increasing rGO content from 8.11%, 25.74%, to 43.47% after freeze-drying, respectively. The SEM images clearly indicate that the rGO are well-dispersed and partially aligned in the PVA matrix. Furthermore, with increasing the loading of rGO, the pore size decreased because the rGO nanosheets are arranged as a 3D network throughout the PVA polymer matrix, and partial hydrogen bonding formed between PVA and rGO. According to a report by Zhao *et al.*,[23] when the loading amount reaches a critical content, rGO nanosheets tend to overlap and restack due to intermolecular forces, such as hydrogen bonding.

3.2. Drug release behavior of the rGO–PVA hydrogels

We used lidocaine hydrochloride, a neutrally charged, low molecular weight, and hydrophilic drug, as a model to study the drug release behavior of the rGO–PVA hydrogels. The natural release behavior of lidocaine hydrochloride from the rGO–PVA hydrogels containing various amounts of rGO was measured over 175 minutes in PBS (pH = 7) (Fig. 3(a)). The accumulated release shown in Fig. 3(a) represents the total amount of drug released from each hydrogel sample. The R0 hydrogel (no rGO), which has a high water uptake and a large pore size (see Fig. 3(b)(i)), displayed a relatively rapid release; approximately 83% of the lidocaine hydrochloride molecules were released within 10 minutes because of strong water uptake. However, the hydrogels with higher rGO loadings exhibited lower release profiles. The R1 sample, which contained 8.11% rGO, lowered the accumulated drug release from 99.9% to 64.2%. Furthermore, for the R5 sample, which contained 43.47% rGO, the accumulated drug release dropped drastically to 35% over 175 minutes. The slower release profiles for the hybrid hydrogels with higher rGO contents were attributed to the dispersion of rGO nanosheets in the polymer matrix to form a 3D network of

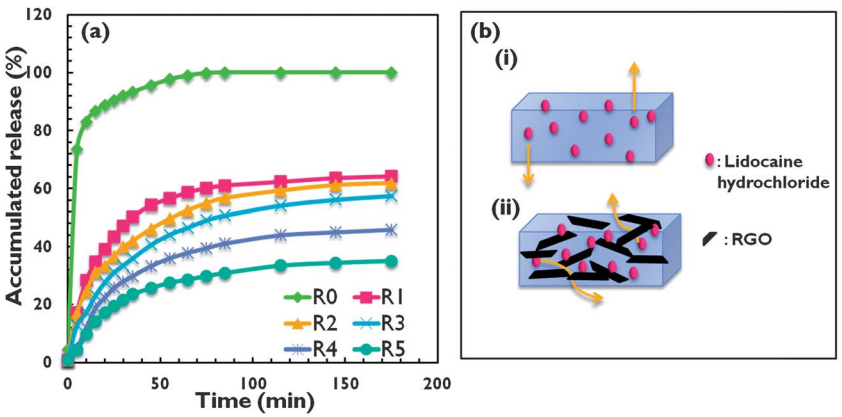

Fig. 3 (a) Natural release of lidocaine hydrochloride from rGO–PVA films of different compositions. (b) Schematic illustration of the natural release of lidocaine hydrochloride from different rGO–PVA hydrogel compositions, (i) without rGO loading and (ii) with rGO loading.

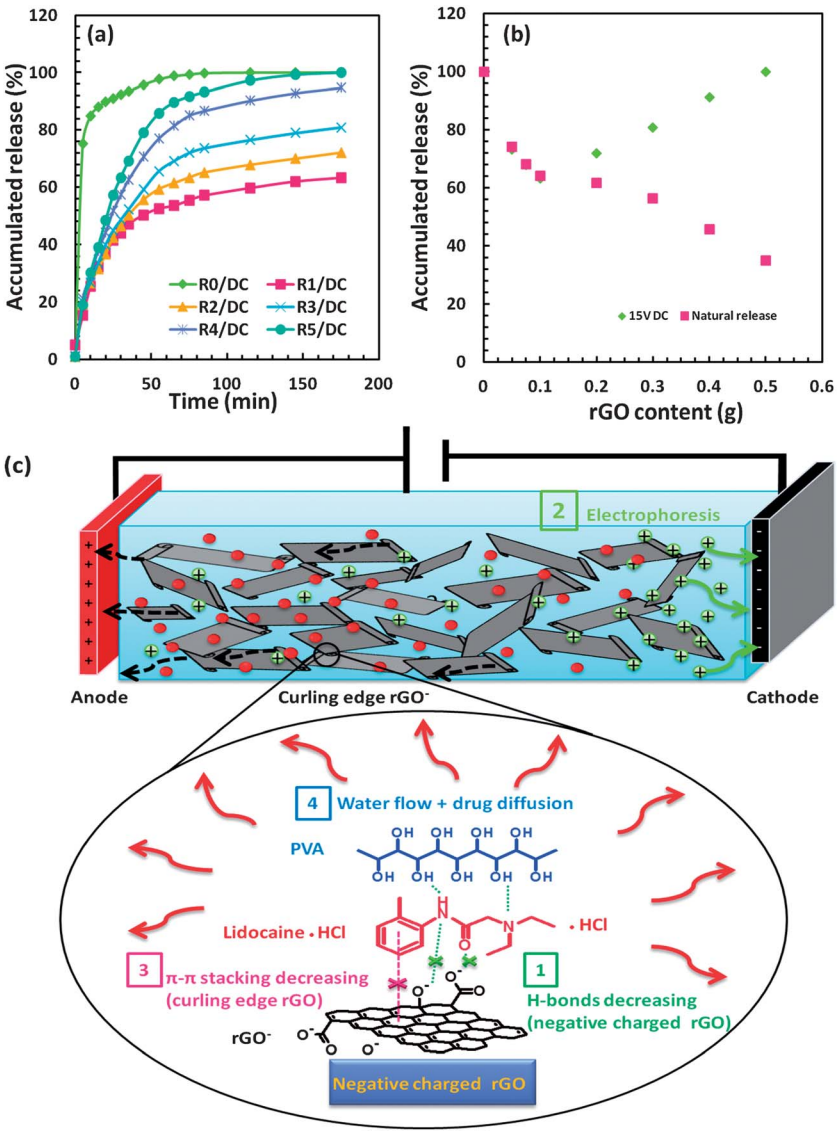

Fig. 4 (a) Time-dependent accumulated release of lidocaine hydrochloride from different compositions of rGO–PVA hydrogels with electrical stimulation at a constant voltage of 15 V. (b) Comparison of the accumulated release of lidocaine hydrochloride occurring naturally and following electrical stimulation at 175 minutes for different rGO contents. (c) Schematic illustration of the controlled release of lidocaine hydrochloride under an electric field.

Table 2 The kinetic constants K and release exponents n determined by the linear regression of lidocaine hydrochloride release from the hydrogels

	Kinetic constant (K)		Release exponent (n)	
	0 V	15 V	0 V	15 V
R0	0.88	0.88	0.78	0.78
R1	0.79	0.77	0.73	0.76
R2	0.71	0.85	0.69	0.79
R3	0.62	0.92	0.64	0.81
R4	0.55	0.96	0.59	0.84
R5	0.52	0.99	0.55	0.88

physical barriers that can efficiently restrict the PVA chain arrangement (defined as a "molecule movement restriction" effect as reported by Bao *et al.*[21]). The PVA chain mobility is extensively inhibited, and rGO distorts the diffusion path (tortuosity) of the lidocaine hydrochloride, as seen in Fig. 3(b)(ii). The increase in the diffusion path throughout the hybrid networks results in a slower drug diffusion. Moreover, with increasing rGO, the pore size decreased, as evidenced by the SEM images in Fig. 2(c)–(e), and the water uptake was also lowered (Table 1, Fig. 3(a)). These data further illustrate that the drug release profiles can be tuned to a certain extent through the manipulation of the chemical composition of the rGO–PVA hybrid hydrogels. To evaluate if the rGO–PVA hydrogel can be applicable to hydrophobic drugs, we chose ibuprofen (206.29 g mol^{-1}) drug to test the release behavior of R5 rGO–PVA hydrogel where the chemical structure of ibuprofen was shown in Fig. S4.† It was found that limited ibuprofen can be loaded into the rGO–PVA hydrogel system because the drug molecule can form π–π stacking interactions with rGO, but electrical

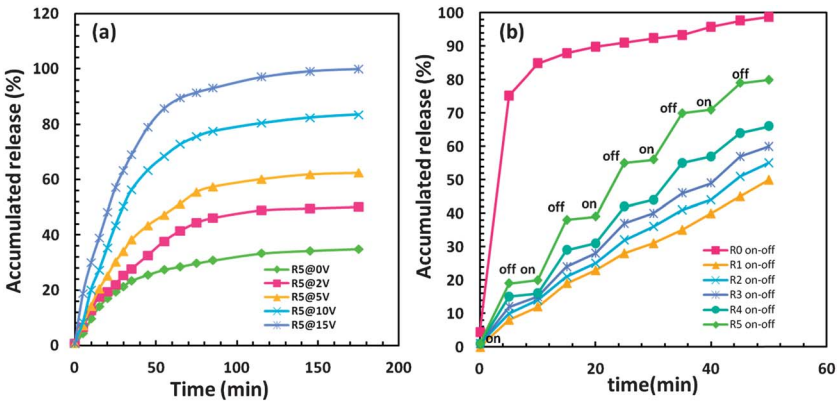

Fig. 5 (a) Time-dependent accumulated release of lidocaine hydrochloride from the R5 hydrogel when a DC electric field set at 0 V, 2 V, 5 V, 10 V, and 15 V was applied. (b) Pulsatile drug release profiles of the different rGO–PVA hydrogels with the application of an electric field of 15 V following on and off switching.

stimulation can still enhance the drug release from 9.1% to 21.5%, indicating that the rGO–PVA hydrogels will be probably applicable for limited hydrophobic drugs. In addition, we also loaded the same amount of vitamin B_{12}, which has a higher molecular weight (1355 g mol^{-1}) than lidocaine hydrochloride, into the R5 rGO–PVA hydrogels to study the drug release behavior. The release behavior of vitamin B_{12} follows the same trend as lidocaine hydrochloride, indicating the rGO–PVA may be applicable for high molecular weight hydrophilic drugs.

3.3. Drug release behavior under an applied electric field

The release profile shown in Fig. 4(a) represents the *in vitro* release behavior of lidocaine hydrochloride from each hydrogel sample at an applied electrical stimulation of 15 V in PBS (pH = 7). Fig. 4(a) demonstrates that the release of lidocaine hydrochloride from the rGO–PVA hydrogels was enhanced by the application of an electrical field. The behaviors were in contrast to those observed in the absence of an electrical stimulus (Fig. 3(a)). The rGO–PVA hybrid hydrogels containing rGO exhibited a large increase in drug release. The cumulative levels of the drug released following electrical stimulation as compared to those naturally released were enhanced by 10.15%, 23.48%, 48.87%, and 64.99% with increasing rGO content for the sample R2, R3, R4 and R5 hydrogels, respectively (Fig. 4(b)). At a constant voltage, the drug release profile of the R0 hydrogel (no rGO) following electrostimulation remained the same as the drug release profile that occurred naturally from the hydrogels; the hybrid hydrogels showed rapid release of lidocaine hydrochloride, which was completely eluted within 15 minutes because of the lack of sufficient physical barriers. In contrast, an enhanced drug release profile was observed for the rGO–PVA hydrogels exposed to the electric field which can be explained as follows: the rGO becomes negative charged because the –COOH of rGO exists as $–COO^-$ and cannot form hydrogen bonds with the –CONH group of lidocaine.[25] The partial dissociation of hydrogen-bonding interactions under basic conditions in Fig. 4(c) would enhance the drug molecule release. Moreover, mobile counter ions, such as Na^+, K^+, and H^+ ions, tend to migrate towards the cathode and drag water and the drug molecules with them. This phenomenon results in an increase in drug release due to electro-osmosis coupled with electrophoresis.[29] Meanwhile, the negatively charged rGO sheets, stuck in the PVA matrix, tend to be pulled towards the anode. If the pulling force is large enough and is allowed to accumulate over time, the morphology of the rGO sheets in the PVA matrix may change (as demonstrated in Fig. 6(c)), *e.g.*, the edges may curl up because of edge defects in the rGO.[30] The morphology changes recorded for the rGO–PVA hydrogels under exposure to identical electrical stimuli (the same voltage) for different time periods are evidenced in the SEM images in Fig. 6. This would decrease the molecular interactions of lidocaine and edge rGO and then increase the lidocaine release. Therefore, as more rGO is incorporated, the rGO–PVA polymeric network becomes more negatively charged, which enhances the action of electro-osmosis and decreases the intermolecular interactions between rGO and lidocaine and results in a faster lidocaine release rate.

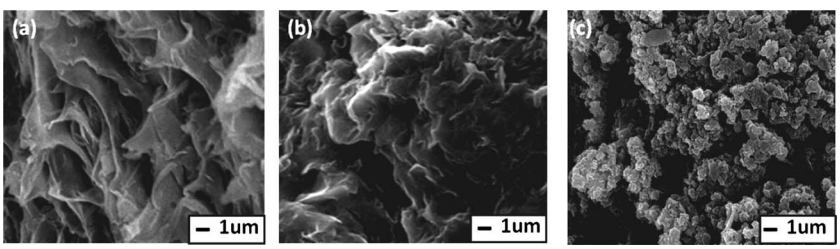

Fig. 6 The cross-sectional morphology of the rGO–PVA R5 hydrogel (a) without stimulation, (b) after 1 h stimulation, and (c) after 3 h stimulation at 15 V.

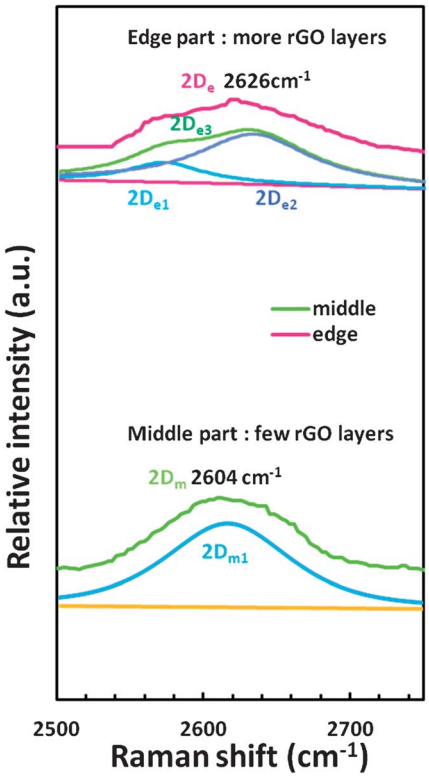

Fig. 7 Raman spectrum recorded at the middle and edge positions of the rGO. The curve $2D_e$ means the original spectrum (without curve fitting) at the edge part of rGO, while the curve $2D_m$ shows the original spectrum in the middle of rGO. The fit of the $2D_{e1}$ and $2D_{e2}$ components of the $2D_{e3}$ band at the edge rGO is shown. The curve $2D_m$ is composed of a single $2D_{m1}$ fitting curve.

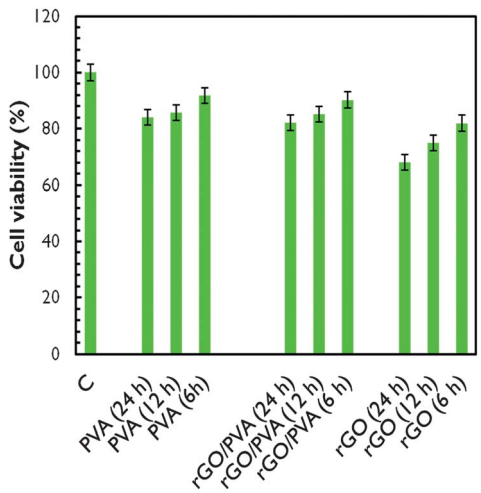

Fig. 8 Cell viability of WS1 cells after 6 h, 12 h, and 24 h incubation with PVA, rGO–PVA, and rGO.

Furthermore, it was noted in Fig. 4(b) that the electrically stimulated drug release of sample R1 exhibited a slight reduction (0.94%) in drug release compared to that without electrical stimulation. This result may be related to the percolation threshold of rGO. When the rGO content is below 8.11%, as shown in Fig. S5† for the rGO–PVA hydrogels with 4% and 6% rGO loading, the electrical stimulation did not exhibit an enhancement in the drug release amount, indicating the negligible difference between the natural and stimulated release amount for the hydrogel with an rGO loading below 8.11%. This implies that when the rGO content is below 8.11%, the exfoliated rGO nanosheets are individually dispersed in the matrix and the tortuosity effect outweighed the electro-induced behaviors in the rGO–PVA matrix. These data suggest that there exists a critical rGO content for enhancing drug release in rGO–PVA hybrid systems.

To further investigate the release of the drug from these rGO–PVA hydrogels, the drug release kinetics were analyzed using the diffusion exponent n and the rate constant, K, as indicated by eqn (1).

$$\frac{M_t}{M_\infty} = Kt^n \quad (1)$$

where M_t is the amount of drug released at time t, M_∞ is the amount of drug released in the equilibrium state, K is a rate constant and n is a diffusion exponent related to the diffusion mechanism. According to the plot of $\ln(M_t/M_\infty)$ *versus* $\ln(t)$, the kinetic parameters were obtained and are shown in Table 2. The K value for natural release decreased with increasing rGO but when the electric field was applied, a larger K value was obtained which implied that the release rate was increased. A similar trend was observed for the release behavior of lidocaine hydrochloride from the hydrogels. The n value decreased from 0.78 to 0.55 as the rGO content increased from R0 to R5 in the absence of an applied voltage, indicating that higher rGO content increased the physical barrier density, and restricted the diffusion of drug molecules. However, an electrical stimulus induced the structural deformation of the rGO–PVA hydrogels, causing an increase in the n value of the R5 hydrogel from 0.55 to 0.88 under an electrical stimulus of 15 V; this release behavior is known as non-Fickian diffusion.[31]

Fig. 5(a) shows the time-dependent accumulated release of lidocaine hydrochloride from the R5 hydrogel under an applied electric field at different DC voltages (0 V, 2 V, 5 V, 10 V, and 15 V) where the amount of drug released from the hydrogel increased with an increase in applied voltage. Compared to the drug release behaviors of electrically responsive hydrogels reported in the literature, where the cumulative drug release ranged from 4.7–25.2% with stimulation for one hour at 5 V,[11] the chip-like rGO–PVA hybrid hydrogels provide a faster response to electrostimulation. The results may be interpreted as follows: (1) the morphology and charge change of the rGO sheets in the PVA matrix can reduce the intermolecular interactions of rGO and lidocaine. Thus, a higher level of drug release is observed under an electric field. (2) The electro-osmosis coupled with electrophoresis of the rGO–PVA hydrogel can cause the drug molecules to diffuse out of the hydrogel. This result suggests that the negatively charged rGO nanosheets are predominately pulled and promoted by larger electric fields. In this study, we also examined the electric sensitivity by subtracting the natural release rate (R_N) from the electrically stimulated release rate (R_E) under an applied voltage at a short time-period stimulus, as shown in Fig. S6.† The sensitivity can be also considered as the responsive behavior of drug release. The release rate was calculated from the slope of the accumulated release profiles. For the

hydrogels with an rGO loading below 8.11% (region A), the electrical sensitivity is relatively low, indicating little sensitivity to a given electrical stimulation. However, in region B (above 8.11%), the sensitivity increases obviously with rGO content. The R5 hybrid hydrogel displays a maximum electrical sensitivity while subjected to an electrical field. In addition, it was also found in Fig. S7† that the sensitivity of the R5 rGO–PVA hybrid hydrogel increased from 1.8% per min to 4.7% per min with an applied voltage from 2 V to 15 V and almost followed a linear relationship, indicating that the drug release can be well controlled even at a lower voltage with minute electrical stimulation. Sustained drug release from the R5 hydrogel can be obtained under a stimulation of 2 V. That is the reason why the R5 rGO–PVA hybrid hydrogel shows highly responsive behavior.

The drug-eluting profiles for various rGO–PVA hybrid hydrogels at various time intervals following repeated on–off electric operation are shown in Fig. 5(b). In the presence of electrical induction, rapid-drug elution from the structure was observed for the R0 hydrogel in the form of a burst-like profile. With greater rGO loading, the amount of drug eluted at each time interval increased; however, a more stepwise change in the profile was observed, particularly for the R4 and R5 hydrogels. From our understanding, the release profile is essentially the consecutive outward diffusion behavior of the drug from the inside of the chip-like structure. The burst-to-zero-to-burst release pattern can be repeated several times, which suggests the following: (1) the nanostructural perturbation of the rGO nanosheets because of electrical induction should be small enough, (2) the mechanical fatigue of the building materials can be effectively reduced, and (3) the chip-like structure is working as a multiple-use drug delivery device capable of delivering drugs with a tunable release profile.

Fig. 6 illustrates the cross-section SEM images of the R5 rGO–PVA hydrogel with/without electric field stimulation after freeze-drying. An electrical stimulus of 15 V was applied to the samples for varying times. After electrical stimulation, the cross-section morphology of the freeze-dried rGO–PVA hydrogels (Fig. 6(b)) changed significantly compared to those without electrostimulation (Fig. 6(a)). This variation in structural morphology implies that the negatively charged rGO nanosheets had the tendency to move towards the anode under the electric field, but they were immobilized by the polymer matrix. Furthermore, when stimulated for a long period (3 h) to increase the driving force, the rGO nanosheets were compressed and distorted by edge defects that caused curling, as seen in Fig. 6(c). Similar curling behavior was reported by Li *et al.*,[30] who showed that morphology changes in graphene can be modified by chemical environments and scrolling from the edges.

The Raman spectrum peak of the 2D band may change in shape and position for the different layers of rGO;[32] therefore, Raman spectroscopy was used to analyze the layers of rGO after stimulation. Fig. 7 shows the Raman spectrum of each rGO nanosheet at different locations, ranging from the edge to the middle, after electrical stimulation of the R5 membrane for 2 h. The rGO nanosheets were taken out by removing the PVA and then dispersed in DI water to separate each rGO nanosheet. In Fig. 7, the curve $2D_e$ indicates the original Raman spectrum (without curve fitting) at the edge part of rGO, while the curve $2D_m$ shows the original Raman spectrum in the middle of rGO. It was found that the $2D_m$ peak position in the middle of an rGO nanosheet was 2604 cm^{-1} but shifted to 2626 cm^{-1} ($2D_e$) at the edge of the rGO. Some studies also report that higher numbers of layers of graphene increase the wave number position of the 2D peak.[28,33–35] In addition, we clearly observed that the $2D_e$ band at the edge of rGO was broader than that in the middle of rGO. According to a report by Ferrari *et al.*,[32] the 2D band of one layer of graphene becomes significantly sharper than higher numbers of layers of graphene which have more fitting curve components to cause a broader peak. After curve fitting, the $2D_{e3}$ band at the edge of rGO can be separated into two components of the $2D_{e1}$ (peak position: 2580 cm^{-1}, corresponding to a phonon of wave vector q1 (ref. 36)) and $2D_{e2}$ (peak position: 2627 cm^{-1}, corresponding to a phonon of wave vector q2 (ref. 36)). The asymmetric 2D band consists of two sub-bands, corresponding to two permissible transition processes in the spectrum of the graphene[37–39] at the edge. Therefore, the results in Fig. 7 suggest that more rGO layers are at the edge due to curling and folding after electrical stimulation in the PVA matrix. From the SEM images and the Raman spectral data shown in Fig. 6 and 7, respectively, the mechanism of the electrically stimulated drug release behavior of the rGO–PVA hydrogel could be deduced.

Fig. 8 shows the results of the MTT assay, which measures the metabolic competence of the WS1 human skin fibroblastoid cell line following incubation with PVA, R5 rGO–PVA, and rGO at a concentration of 6.25 mg ml^{-1}. The result also indicates that the difference in the cytotoxicity of the rGO–PVA at 6 h, 12 h, and 24 h incubation is negligibly small. After 24 h incubation with rGO–PVA, the cell viability still can remain above 80%. The results from the MTT assay suggest that the rGO–PVA has low toxicity with respect to the WS1 cell line and is suitable for the fabrication of electrically stimulated membranes for controlled drug release.

4. Conclusion

In this study, a hydrogel composed of PVA and inorganic rGO was assembled into a chip-like membrane to study its electrically modulated drug release behavior *in vitro* using lidocaine hydrochloride as a model drug molecule. The membranes display a faster response to electrostimulation and provide a number of electrically modulated drug release profiles *in vitro*, which range from a burst-like pattern to a slow-elution pattern, through the manipulation of the chemical composition of the rGO nanosheets in the PVA matrix. In addition, consecutive repeated "on" and "off" operations show that the electric responsiveness and reliability of the electrically modulated hydrogel was considerably improved with higher rGO content. This new class of hybrid hydrogels provides an interesting alternative as a long-standing, electrically induced drug delivery system with reliable and responsive drug release performance. The rGO–PVA hydrogel *in vivo* study will be published elsewhere to demonstrate that the rats survived safely with no side effects detected after the tests. Our data strongly support our hypothesis that by incorporating inorganic, conductive and biocompatible reduced graphene oxide within a hydrogel can successfully bypass the traditional limitations of electrically responsive hydrogels.

Acknowledgements

This work was financially supported by the National Science Council of the Republic of China, Taiwan under Contract of NSC 99-2221-E-009-070-MY3 and NSC 99-2113-M-009-013-MY2. This work is also supported by "Aim for the Top University Plan" of the National Chiao Tung University and Ministry of Education, Taiwan, R.O.C.

References

1 P. Gupta, K. Vermani and S. Garg, *Drug Discovery Today*, 2002, **7**, 569–579.
2 T. Y. Liu, S. H. Hu, K. H. Liu, D. M. Liu and S. Y. Chen, *J. Controlled Release*, 2008, **126**, 228–236.
3 J. Ge, E. Neofytou, T. J. Cahill, R. E. Beygui and R. N. Zare, *ACS Nano*, 2011, **6**, 227–233.
4 X. Luo, C. Matranga, S. Tan, N. Alba and X. T. Cui, *Biomaterials*, 2011, **32**, 6316–6323.
5 T. Mirfakhrai, J. D. W. Madden and R. H. Baughman, *Mater. Today*, 2007, **10**, 30–38.
6 C. Wang, A. Javadi, M. Ghaffari and S. Gong, *Biomaterials*, 2010, **31**, 4944–4951.
7 M. R. Abidian, D. H. Kim and D. C. Martin, *Adv. Mater.*, 2006, **18**, 405–409.
8 D. Svirskis, J. Travas-Sejdic, A. Rodgers and S. Garg, *J. Controlled Release*, 2010, **146**, 6–15.
9 C. J. Whiting, A. M. Voice, P. D. Olmsted and T. C. B. McLeish, *J. Phys.: Condens. Matter*, 2001, **13**, 1381–1393.
10 M. Sudaxshina, *J. Controlled Release*, 2003, **92**, 1–17.
11 T. S. Tsai, V. Pillay, Y. E. Choonara, L. C. Du Toit, G. Modi, D. Naidoo and P. Kumar, *Polymers*, 2011, **3**, 150–172.
12 K. H. Liu, T. Y. Liu, S. Y. Chen and D. M. Liu, *Acta Biomater.*, 2008, **4**, 1038–1045.
13 W. C. Huang, T. J. Lee, C. S. Hsiao, S. Y. Chen and D. M. Liu, *J. Mater. Chem.*, 2011, **21**, 16077–16085.
14 Y. Qiu and K. Park, *Adv. Drug Delivery Rev.*, 2001, **53**, 321–339.
15 H. Bai, C. Li, X. Wang and G. Shi, *Chem. Commun.*, 2010, **46**, 2376–2378.
16 B. Lu, T. Li, H. Zhao, X. Li, C. Gao, S. Zhang and E. Xie, *Nanoscale*, 2012, **4**, 2978–2982.
17 H. J. Salavagione, G. Martinez and M. A. Gomez, *J. Mater. Chem.*, 2009, **19**, 5027–5032.
18 J. H. Yang and Y.-D. Lee, *J. Mater. Chem.*, 2012, **22**, 8512–8517.
19 H. A. Becerril, J. Mao, Z. Liu, R. M. Stoltenberg, Z. Bao and Y. Chen, *ACS Nano*, 2008, **2**, 463–470.
20 C. M. Hassan and N. A. Peppas, *Macromolecules*, 2000, **33**, 2472–2479.
21 C. Bao, Y. Guo, L. Song and Y. Hu, *J. Mater. Chem.*, 2011, **21**, 13942–13950.
22 Y. Xu, W. Hong, H. Bai, C. Li and G. Shi, *Carbon*, 2009, **47**, 3538–3543.
23 X. Zhao, Q. Zhang, D. Chen and P. Lu, *Macromolecules*, 2010, **43**, 2357–2363.
24 J. Liang, Y. Huang, L. Zhang, Y. Wang, Y. Ma, T. Guo and Y. Chen, *Adv. Funct. Mater.*, 2009, **19**, 2297–2302.
25 X. Yang, X. Zhang, Z. Liu, Y. Ma, Y. Huang and Y. Chen, *J. Phys. Chem. C*, 2008, **112**, 17554–17558.
26 X. Sun, Z. Liu, K. Welsher, J. Robinson, A. Goodwin, S. Zaric and H. Dai, *Nano Res.*, 2008, **1**, 203–212.
27 C. Y. Su, Y. Xu, W. Zhang, J. Zhao, X. Tang, C. H. Tsai and L. J. Li, *Chem. Mater.*, 2009, **21**, 5674–5680.
28 S. Stankovich, D. A. Dikin, R. D. Piner, K. A. Kohlhaas, A. Kleinhammes, Y. Jia, Y. Wu, S. T. Nguyen and R. S. Ruoff, *Carbon*, 2007, **45**, 1558–1565.
29 A. Kikuchi and T. Okano, *Adv. Drug Delivery Rev.*, 2002, **54**, 53–77.
30 Q. Li, Z. Li, M. Chen and Y. Fang, *Nano Lett.*, 2009, **9**, 2129–2132.
31 M. Lee, J.-W. Nah, Y. Kwon, J. J. Koh, K. S. Ko and S. W. Kim, *Pharm. Res.*, 2001, **18**, 427–431.
32 A. C. Ferrari, J. C. Meyer, V. Scardaci, C. Casiraghi, M. Lazzeri, F. Mauri, S. Piscanec, D. Jiang, K. S. Novoselov, S. Roth and A. K. Geim, *Phys. Rev. Lett.*, 2006, **97**, 187401.
33 V. Singh, D. Joung, L. Zhai, S. Das, S. I. Khondaker and S. Seal, *Prog. Mater. Sci.*, 2011, **56**, 1178–1271.
34 I. Calizo, A. A. Balandin, W. Bao, F. Miao and C. N. Lau, *Nano Lett.*, 2007, **7**, 2645–2649.
35 J. S. Park, A. Reina, R. Saito, J. Kong, G. Dresselhaus and M. S. Dresselhaus, *Carbon*, 2009, **47**, 1303–1310.
36 D. Graf, F. Molitor, K. Ensslin, C. Stampfer, A. Jungen, C. Hierold and L. Wirtz, *Nano Lett.*, 2007, **7**, 238–242.
37 P. Poncharal, A. Ayari, T. Michel and J. L. Sauvajol, *Phys. Rev. B: Condens. Matter Mater. Phys.*, 2008, **78**, 113407.
38 K. Yan, H. Peng, Y. Zhou, H. Li and Z. Liu, *Nano Lett.*, 2011, **11**, 1106–1110.
39 L. M. Malard, M. A. Pimenta, G. Dresselhaus and M. S. Dresselhaus, *Phys. Rep.*, 2009, **473**, 51–87.

